Stabilization of quercetin flavonoid in MCM-41 mesoporous silica: positive effect of surface functionalization

Stabilization of quercetin flavonoid in MCM-41 mesoporous silica: positive effect of surface functionalization

Gloria Berlier[1], Lucia Gastaldi[2], Elena Ugazio[2], Ivana Miletto[1], Patrizia Iliade[1], Simona Sapino[2*]

[1] Dipartimento di Chimica, Università degli Studi di Torino and NIS, Nanostructured Interfaces and Surfaces Centre of Excellence, Via P. Giuria 7, 10125 Torino, Italy

[2] Dipartimento di Scienza e Tecnologia del Farmaco, Università degli Studi di Torino, Via P. Giuria 9, 10125 Torino, Italy

[*] Corresponding author:

Tel: +39 (0)116707686; Fax: +39 (0)116707687; e-mail: simona.sapino@unito.it

Abstract

Antioxidants can prevent UV-induced skin damage mainly by neutralizing free radicals. For this purpose quercetin (Q) is one of the most employed flavonoid even if the potential usefulness is limited by its unfavorable physico-chemical properties. In this context mesoporous silica (MCM-41) is herein proposed as a novel vehicle able to improve the stability and performance of this phenolic substrate in topical products. Complexes of Q with plain or octyl-functionalized MCM-41 were successfully prepared with different weight ratios by a kneading method and then they were characterized by XRD, gas-volumetric (BET), TGA, DSC and FTIR analyses. The performances of the different complexes were evaluated *in vitro* in terms of membrane diffusion profiles, storage and photostability, antiradical and chelating activities.

The physico-chemical characterization confirmed an important host/guest interaction due to the formation of Si-OH/quercetin hydrogen bonded adducts further strengthened by octyl functionalization through van der Waals forces. The immobilization of Q, particularly on octyl-fuctionalized silica, increased the stability without undermining the antioxidant efficacy opening the way for an innovative employment of mesoporous composite materials in the skincare field.

Keywords: quercetin; MCM-41; octyl-functionalization; kneading; stability; topical application

1 Introduction

Oxidative stress has been one of the most widely studied biochemical processes and is the consequence of an imbalance between pro- and antioxidant species. The former essentially concerns highly reactive oxygen or nitrogen species (ROS or RNS) [1] that can lead to the oxidation of lipids, proteins or nucleic acids and contribute to cellular dysfunctions [2]. To avoid oxidative stress, cells are equipped with two major antioxidant defense systems. The first concerns enzymes which catalyze ROS or RNS degradation, while the second involves antioxidants like vitamins A, C, E and glutathione, which act by redox reactions [3,4]. Flavonoids have recently attracted a great interest as potential reducing agents, hydrogen-donating antioxidants and singlet oxygen quenchers; in some cases metal chelating properties have also been proposed [5,6]. Quercetin, in particular, satisfies all the proposed criteria for effective radical scavenging, since the o-dihydroxy-structure in the B ring (Scheme 1) confers high stability to the radical form and participates in electronic delocalization [7]. The therapeutic usefulness of these potential benefits is, however, limited by the unfavorable physico-chemical properties of this compound, especially its very poor water solubility and low stability.

A recently proposed strategy to protect labile compounds from photodegradation and to improve their solubility in pharmaceutical formulations consists in their inclusion in supramolecular structures characterized by the presence of cavities where the molecule can diffuse. Examples of this approach involve phospholipid pockets [8,9], nanostructures [10], cyclodextrin cage holes [11,12], interlamellar voids in hydrotalcite layered structures [13,14] or cylindrical pores in ordered mesoporous silica matrices [15-18].

The interest for ordered mesoporous silica is related to the well known properties of this class of materials, including high surface areas (as high as 1000 m^2/g), tunable pore size (20-300 Å), ordered and robust porosity allowing the diffusion of bulky molecules, thermal stability, biocompatibility [19,20] and the possibility to tune the hydrophilic silica character by surface functionalization either during (co-condensation) or after the synthesis (grafting) [21,22]. The great

versatility of these materials testifies their wide variety of applications: as sensors and bio-sensors for the recognition of target molecules [23], in bio-catalysis [24-28], drug delivery [20,29] and bio-imaging [30-32].

In particular, pharmaceutical application research on mesoporous silica has received great attention in the last few years. However, as we understand, few studies are reported about its use in topical products and anyway they concern UV-filters [15,33].

Thus, this work reports on the immobilization of quercetin in MCM-41 mesoporous silica: different complexes have been prepared by a kneading method [34], varying the quercetin/silica weight ratios. Notably, this technique has been recently proposed to prepare complexes with cyclodextrins [35] but until now any references reported its employment with mesoporous matrices. Herein, the same approach is employed on MCM-41 functionalized with octyl groups, to vary the hydrophobic/hydrophilic character of the surface. The resulting materials are characterized about their physico-chemical features and tested about the release of quercetin from the complexes. The results are discussed in terms of the interaction of quercetin with the silica surface in particular after the dispersion in a colloidal system (O/W emulsion) representative of dermal preparations. To demonstrate the possible employment of this inorganic carrier for skin applications, the model complex (quercetin/MCM-41) is investigated for stability also in the presence of a photocatalyst (TiO_2), frequently used in sunscreen lotions as a broad-band UV-filter. Besides the antioxidant activity of the mesoporous composite material is assessed and compared with raw quercetin.

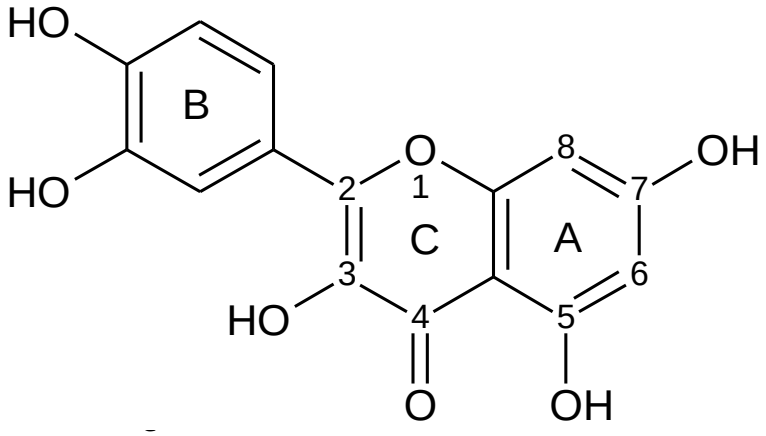

Scheme 1. Structure of quercetin molecule

2 Experimental Section

2.1 Materials

Acetone, absolute ethanol, methanol, citric acid trisodium salt were purchased from Carlo Erba. Acetic acid, hydrochloric acid, monosodium phosphate, disodium phosphate, ferrozine (3-(2-pyridyl)-5,6-diphenyl-1,2,4-triazine-4',4''-disulfonic acid sodium salt, iron(II)sulfate were purchased from Fluka.

Anhydrous citric acid, dimethicone (Abil 350), glycerin, imidazolidinyl urea (Kemipur 100), octyl octanoate (Tegosoft EE) were products ACEF. Carbomer (Carbopol ETD 2001) was from Noveon. Titanium dioxide (Degussa P 25) was a product Degussa. DPPH$^{\bullet}$ (2,2-diphenyl-1-picrylhydrazyl free radical), quercetin (Q), n-cetyltrimethylammonium bromide (CTAB), silica (SiO_2), n-octyl triethoxysilane, and toluene were purchased from Sigma-Aldrich. Potassium palmitoyl hydrolyzed wheat protein/ glyceryl stearate/ cetearyl alcohol (Phytocream 2000) was a product Sinerga. Esters of 4-hydroxybenzoic acid in 2-phenoxyethanol (Uniphen P-23) was from Induchem.

2.2 Synthesis

Purely siliceous mesoporous MCM-41 (hereafter M) was synthesized according to literature using SiO_2 in basic conditions and CTAB as Structure Directing Agent (SDA) [19,36]. After a hydrothermal treatment in autoclave, the white obtained product was filtered, washed with abundant filtered water, dried in oven at 100 °C for one night and finally calcined in nitrogen and oxygen atmosphere at 600 °C.

MCM-41 functionalized with octyl groups (octM) was prepared by suspending 0.5 g of calcined M in 30 mL of toluene. 0.8 mL of n-octyl triethoxysilane were added drop wise and the mixture was allowed to reflux for 8 h. The reaction solution was centrifuged and the deposited gel washed with ethanol and deionized water. The obtained white solid was filtered, washed with methanol and dried *in vacuum*.

Inclusion complexes of quercetin (Q) in mesoporous MCM-41 silica (M or octM) were prepared by the kneading method [35] in 1/2, 1/4 and 1/8 weight ratios. A homogeneous paste was made by mixing in a mortar Q (33.0, 20.0 or 11.1 mg) with 250 µL of acetone. An opportune amount of silica was added and the mixture was kneaded until complete acetone evaporation (about 10 min). Resulting samples are hereafter labeled as QM_1/X and QoctM_1/X (X = 2, 4 or 8). Physical mixtures were prepared with the same weight ratios by simple blending in vials, giving samples PhMix_1/X.

2.3 Physico-chemical characterization

Powder X Ray Diffraction (XRD) patterns were collected on a X'Pert Pro Bragg Brentano diffractometer (Philips) using Cu Kα radiation (40 mA and 45 kV), with a scan speed of 0.01° min^{-1}.

Gas-volumetric analysis (N_2 adsorption–desorption isotherms at liquid nitrogen temperature, LNT) was employed to measure specific surface area (SSA), pore volume and size with a ASAP 2020 (Micromeritics). SSA was calculated by the Brunauer, Emmet, Teller (BET) method, whilst average

pore size and volume were estimated by the Barret, Joyner, Halenda – Kruk, Jaroniec, Sayari (BJH-KJS) method [37]. For the latter the Kruk-Jaroniec-Sayari equations were employed in the adsorption isotherms. Prior to analyses, the samples were outgassed overnight at room temperature (RT).

Thermal gravimetric analysis (TGA) was carried out on a TAQ600 (TA Instruments) heating the samples at a rate of 10 °C from RT to 1000 °C in a nitrogen flow. Before starting the measurements, the samples were flushed in N_2 at RT for 15 min and equilibrated at 30 °C. Once reached the final temperature an isotherm was run for 15 min in air.

Differential scanning calorimetry (DSC) analyses were performed on a DSC-7 power compensation thermal analyzer (Perkin Elmer), performing temperature calibration with indium as standard. 3-6 mg of samples having the same amount of Q were loaded in aluminum pans and heated under nitrogen flow at a scanning speed of 10 °C min^{-1} from 100 to 350 °C.

Q loading was determined with a DU 730 UV/Vis Spectrophotometer (Beckman Coulter) working at a wavelength of 371 nm. A weighed amount of each complex was dispersed in methanol, centrifuged and spectrophotometrically measured. Calibration curves were obtained in different media with diluted Q solutions over the range 1.5×10^{-5}-15.2×10^{-5} M. The molar extinction coefficients (ε) were 21290 M^{-1} (R^2 = 0.9915) in methanol, 18380 M^{-1} (R^2= 0.9995) in methanol/water (30/70 v/v), 21450 M^{-1} (R^2= 0.9992) in ethanol/water (30/70 v/v).

For HPLC analysis a system (Shimadzu) consisting of a LC-6A pump unit control, a SPD-2A UV-Vis detector, a C-R3A chromatopac integrator and a RP-C18 column (Waters, 150×4.6 mm; 5 µm) was employed. The mobile phase was a mixture of methanol/water/acetic acid (50/47/3 v/v/v) with flow rate of 0.8 mL/min. The elution profile was monitored at 371 nm and the retention time of Q was about 4.5 min. The amount of Q in the sample expressed as Q loading percentage (% Q) was quantified, based on the standard curve generated by calculating HPLC peak area of pure Q ($y = 21530\ x + 0.003$, R^2= 0.9999). Each quantified datum was averaged from triplicate analysis. In addition the efficiency of encapsulation (% EE) was calculated as follows:

$$\% \text{ EE} = (\text{Total amount of loaded Q}/\text{Total amount of used Q}) \times 100$$

Fourier transform infrared spectra were recorded using a FTIR-5300 spectrometer (Jasco) equipped with a DTGS detector, working with resolution of 4 cm^{-1} over 32 scans. Samples were in the form of self-supporting pellets suitable for transmission IR experiments and were placed in a quartz cell equipped with KBr windows, designed for RT studies *in vacuum* and controlled atmosphere. Before FTIR analyses the samples were outgassed at RT to remove physically adsorbed water and impurities.

2.4 Testing of complex properties

Q release was evaluated employing a diffusion apparatus consisting of two horizontal glass cells each of 23 mL volume separated by a Spectra/Por (12000-14000 MWCO) hydrophilic cellulose membrane (Spectrum Lab). The available diffusion area of cell was 3.14 cm^2 area. The donor phase consisted of ethanol/citrate buffer mixture (30/70 v/v) at pH 5.0 containing 0.125 mM Q, free or immobilized on silica at different w/w ratios, while the receiving phase was ethanol/citrate buffer mixture (30/70 v/v) at pH 5.0. At fixed times up to 24 h, an aliquot (1.0 mL) of the receiving phase was withdrawn, replaced with an equal volume of fresh medium, suitably diluted and analyzed using the HPLC method described previously. The experiment was carried out in triplicate.

Photodegradation runs were carried out in triplicate, by irradiating the systems listed below, by a G40T10E UVB lamp (Sankyo Denki) with 2.5×10^{-4} W cm^{-2} power irradiance from a distance of 10 cm. During irradiation the samples were stirred by a RO 5 multiple magnetic stirrer (IKA). At scheduled times up to 3 h, a fixed amount (200 µL) of each sample was withdrawn and properly diluted with methanol for spectrophotometrical analysis. The photodegradation kinetics were studied by plotting the percentage of non degraded Q as a function of irradiation time in min. The percentage of non degraded Q was calculated as follows:

$$\% \text{ non degraded Q} = C_t/C_0 \times 100$$

where C_0 is the Q concentration at zero time while C_t is the Q concentration after a given irradiation time (*t*).

The systems subjected to irradiation study were the following: *i)* ethanol/water (15/85 v/v) mixture containing TiO_2 (0.05% w/w); *ii)* O/W emulsion containing TiO_2 (1.0% w/w), at pH 5.0. In both systems Q, free or immobilized, was dispersed at 0.25 mM final concentration.

The O/W emulsion was prepared by dispersing under SL-2 homogenizer (Silverson) the melted lipid phase (2.5 g Phytocream 2000, 6.5 g Tegosoft EE and 1.0 g Abil 350) in 83.6 g filtered water, separately heated at about 75 °C, containing 0.1 g Carbopol ETD 2001, 4.5 g glycerin and 0.5 g Uniphen P-23. The obtained emulsion was then mechanically stirred while cooling to RT, hence 0.3 g Kemipur 100 and 1.0 g Degussa P 25 were added by homogenizing.

Finally, a weighted amount of Q, either free or complexed, was dispersed in each medium under mechanical stirring, resulting in the same final Q concentration of 0.25 mM. If necessary the pH was adjusted to 5.0 with 0.5 N HCl.

The storage stability of Q in aqueous media at pH 5.0 or 7.4 was investigated. Here samples of Q, QM_1/4 and QoctM_1/4 in ethanol/buffer (15/85 v/v) were prepared employing 0.1 M citrate or phosphate buffer, respectively. An aliquot of each sample (10 mL) was kept sheltered from light under magnetic stirring at 37 ± 1 °C. At scheduled intervals up to 180 min, an amount (150 µL) of samples was withdrawn, properly diluted with methanol and spectrophotometrically analyzed. The experiment was carried out in triplicate.

Antioxidant activity was determined based on the ability of the antioxidants to act as radical scavengers towards the stable 2,2-diphenyl-1-picrylhydrazyl free radical ($DPPH^{\bullet}$). This method previously described by Gulcin [38] was used with slight modifications. Briefly, dilutions (50.0 µl) of Q or complexes (QM_1/4 and QoctM_1/4) in the range 3.0-250.0 µM were added to 3.0 mL of $DPPH^{\bullet}$ saturated ethanol/water (20/80 v/v) solution. Samples were kept under magnetic stirring for 10 min at RT in darkness to reach the steady-state condition; after samples centrifuging, absorbance

readings were taken at 515 nm. The radical scavenging activity (RSA) was determined through the following equation:

$$\% \text{ RSA} = (A_0 - A_x)/A_0 \times 100$$

whereby A_0 is the absorbance of the control (containing DPPH$^{\bullet}$ solution without antioxidant) and A_x is the absorbance in the presence of Q or complexes. Each sample was prepared and analyzed in triplicate and % RSA was plotted against each dilution of Q.

The ability of Q, QM_1/4 and QoctM_1/4 to chelate ferrous ion (Fe^{2+}) was investigated based on the method employed by Dinis *et al*. [39]. In this slightly modified assay, different concentrations of antioxidant (0-35.0 μM) in 4.0 mL ethanol/water solution (20/80, v/v) were incubated with $FeSO_4$ (0.05 mL, 2.0 mM) and ferrozine aqueous solution (0.20 mL, 2.0 mM). After the mixtures had reached equilibrium (10 min of magnetic stirring, RT), their absorbances were measured spectrophotometrically at 562 nm. The ability of each antioxidant to inhibit the formation of the ferrous-ferrozine complex, expressed as its Fe^{2+} chelating effect (% chelating activity), was then calculated using the equation:

$$\% \text{ chelating activity} = [(A_0 - A_x)/A_0] \times 100$$

where A_0 is the absorbance of a solution containing only $FeSO_4$ and ferrozine, while A_x is the absorption of the sample containing the flavonoid. Each sample was prepared and investigated in triplicate.

3 Results and discussion

The reported work summarizes a large set of experiments involving the preparation, characterization and testing of QM_1/X and QoctM_1/X complexes, prepared by kneading method at different organic/inorganic weight ratios (X = 2, 4 or 8). The performances of the different QM and QoctM complexes were tested about diffusion and photostability, while only QM_1/4 and QoctM_1/4 complexes were selected to test the antiradical and chelating activities of complexed Q.

3.1 Physico-chemical characterization

Physico-chemical characterization was carried out to get information about the location of the Q molecules in the mesoporous matrix (inside the pores or on the external surface) and about their interaction with the silica surface. Since this kind of information is not straightforward, a description of the complexes in these terms could be obtained only by putting together pieces of information obtained with different techniques. For sake of brevity, the results description will be focused on the samples with 1/4 weight ratio. The values obtained on the other samples are compared in the corresponding tables, when possible. Some of the techniques were not applied to the samples with 1/8 weight ratio, due to low Q loading.

The XRD patterns of QM_1/4 and QoctM_1/4 complexes are reported in Fig. 1, together with that of samples M and octM for comparison. All samples display the typical (100), (110), (200) and (210) peaks related to a hexagonal network of mesopores (P6mm), with the latter ones suggesting the presence of a long range order. This implies that both grafting and drug loading did not affect the ordered mesostructure. While the peaks position is substantially unaffected by both processes, their intensity decreases in both cases, in the order: M > octM ≅ QM_1/4 > QoctM_1/4. This decrease in intensity can be interpreted as a decrease in the electronic density differences between “empty” pores and “filled” silica walls, suggesting that both octyl moieties and Q molecules were included within the silica pores. Thus, with respect to parent M, pores were partially filled in QM_1/4 and octM samples, and were filled in greater amount in QoctM_1/4.

Figure 1

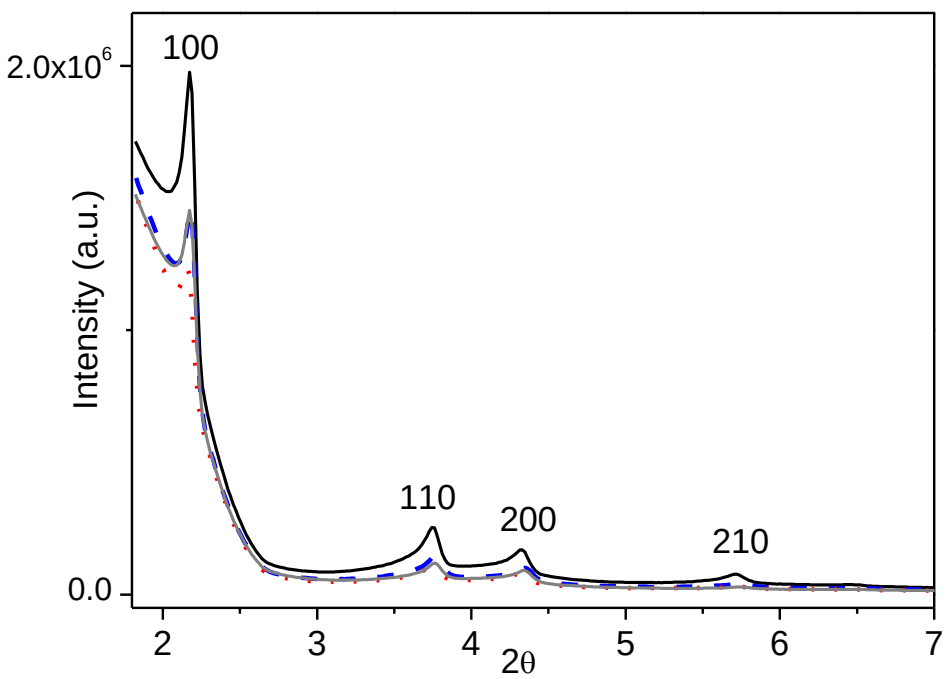

Fig. 1. Low angle powder XRD patterns of M, octM (black and grey full lines, respectively) QM_1/4 and QoctM_1/4 (blue dashed and red dotted lines, respectively).

The results of gas-volumetric analysis of the same 1/4 samples are reported in Fig. 2, with the corresponding M and octM samples for comparison.

Figure 2

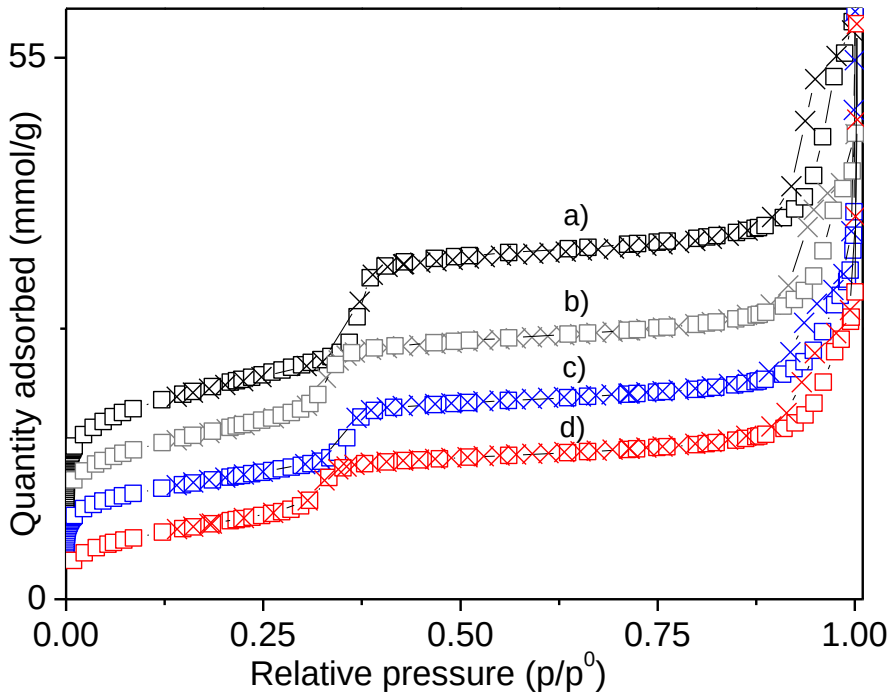

Fig. 2. Nitrogen adsorption isotherm (×) and desorption (□) on: a) M; b) octM; c) QM_1/4; d) QoctM_1/4. Curves were vertically shifted for clarity.

All samples show type IV isotherms with H1 hysteresis loop, typical of mesoporous M samples [30,40]. While the slope at intermediate p/p^0 = 0.35 is an indication of nitrogen capillary condensation inside the mesopores, the H1 type hysteresis loop at high p/p^0, a characteristic of the cylindrical pores open at both ends or of the agglomerates of approximately spherical particles arranged in fairly regular array [41,42], is related to interparticle macroporosity [43,44].

Comparison of the three curves show that SSA decreases in the order M > octM > QM_1/4 ≅ QoctM_1/4, as summarized in Table 1. This change in SSA is accompanied by a decrease in the pores diameter and volume, supporting the hypothesis that Q molecules are included within the pores in both M and octM matrices. However, a decrease of pore volume is also observed in the 200 – 1000 Å range for all samples (pore size centered around 500 Å, that is at the border value between meso- and macropores). This indicates that Q molecules are also stabilized on the external surface

of silica particles, in the interparticle porosity. Finally, by comparing the results obtained with 1/4 and 1/2 ratios (Table 1) it is noticeable that the increase of Q weight ratio does not sensibly affect the changes in area and porosity of bare M matrix, while a major effect is observed in functionalized octM complexes.

Table 1. Porosity and specific surface area of the silica based samples

Samples	Pore diameter[a] (Å)	SSA [b] ($m^2 \cdot g^{-1}$)	Pore volume [c] ($cm^3 \cdot g^{-1}$)	Pore volume [d] ($cm^3 \cdot g^{-1}$)
M	39	1133	0.87	0.63
QM_1/4	38	676	0.55	0.36
QM_1/2	38	624	0.49	0.40
octM	38	890	0.52	0.47
QoctM_1/4	36	651	0.50	0.36
QoctM_1/2	36	489	0.38	0.35

[a] Mean pore diameter calculated by the BJH-KJS method in the adsorption branch. [b] Calculated by the BET method. [c] Calculated by the BJH-KJS method in the 25-50 Å range. [d] Calculated by the BJH-KJS method in the 200-1000 Å range.

TG analysis was employed to measure the final Q loading in the different complexes and to get information on Q interaction with the silica surface before and after octyl functionalization (Fig. 3). The decomposition profiles can be compared with that of pure Q, measured in the same conditions (Fig. 4). The latter shows a main weight loss at 360 °C and a more gradual one at higher temperature (maxima of first derivative at 500 and 600 °C). The first weight loss of free Q (endothermic phenomena) roughly corresponds to 30% weight, compatible with the decomposition of the central C ring or with the loss of one of the two A and B di-hydroxylated rings (scheme 1). The small feature at 320 °C (indicated with a star in Fig. 4) is compatible with the solid/liquid phase transition, in agreement with DSC data (see below).

The decomposition profiles of QM and QoctM complexes can be compared to those of the parent M and octM, for further information on the surface interaction. Firstly, M sample shows a weight loss up to 100 °C, typical of adsorbed water molecules, followed by a smooth weight decline up to 1000 °C, related to surface dehydroxylation [45]. This also holds for all complexes and for octM, where an additional feature (between 100 and 600 °C) is related to the octyl functionalities. In addition to these features, both QM and QoctM complexes show a decomposition profile similar to that of free Q, but in this case the first weight loss is less steep and shifted to lower temperature (around 260 °C in QM_1/4). This suggest that the interaction of Q molecules with the silica surface affects its thermal stability.

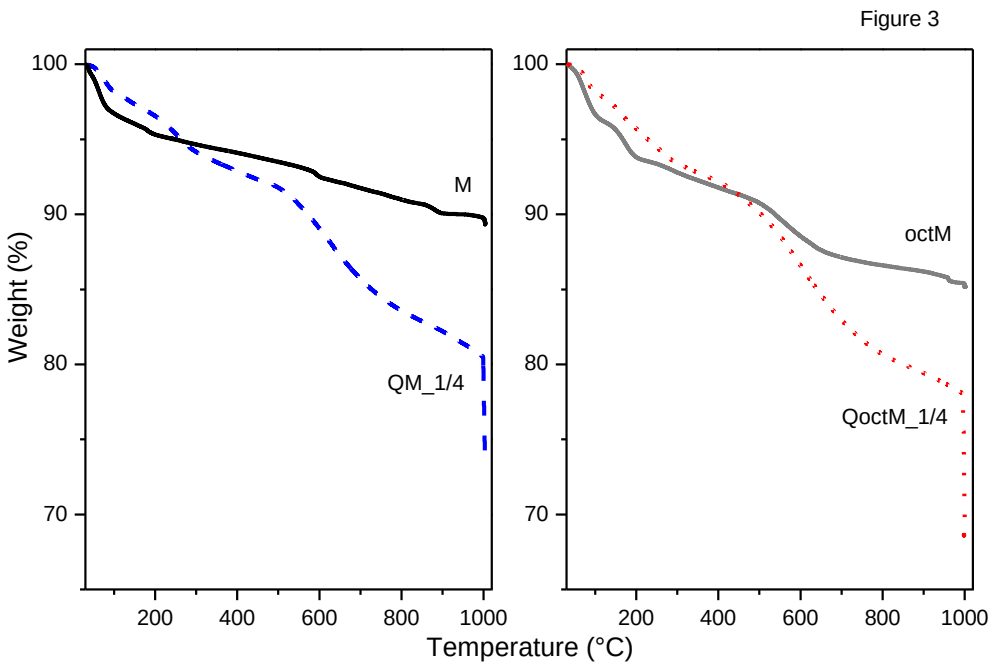

Fig. 3. Thermogravimetric analysis of M and QM_1/4 (left), octM and QoctM_1/4 (right). Weight losses were measured in N_2 flow up to 1000 °C, and in air for a 15 min isotherm at the same temperature.

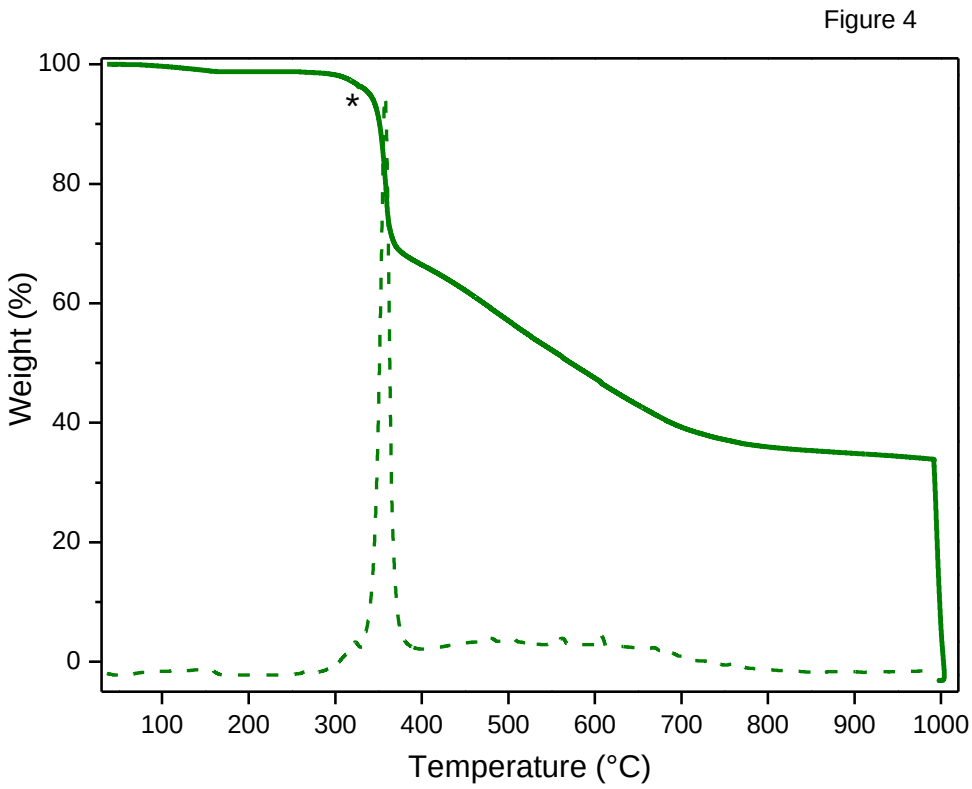

Fig. 4. Thermogravimetric analysis (ramp in N_2 and isotherm in air) of pure Q and corresponding weight derivative (full and dashed curves, respectively). The star indicates the solid/liquid phase transition also monitored by DSC.

Coming to quantitative considerations, a decrease in adsorbed water after Q inclusion in all samples (see also Table 2) is observed, together with a minor extent of dehydroxylation. The latter was arbitrarily estimated from weight loss in the 800–1000 °C range. Q loading was thus calculated from the total weight loss, after subtraction of the alleged contribution from adsorbed water and dehydroxylation. The calculation included the weight loss during the isotherm in air (vertical decrease at 1000 °C), aimed at burning out carbonaceous residues formed as a consequence of organic pirolysis in nitrogen flow. Obviously, in the case of QoctM the contribution due to octyl functional groups (9.5 wt.%) was also subtracted.

Table 2. Data from thermogravimetric analysis (percentage weight loss) and from UV-Vis spectrophotometric analysis (percentage of loading, % Q and efficiency of encapsulation, % EE)

			Quercetin		
Samples	Water [a]	Hydroxyl groups [b]	TGA [d]	% Q [e]	% EE [e]
M	3.3	7.4	-		
QM_1/2	1.2	3.8	33.0	28.0	84.0
QM_1/4	1.8	3.8	21.0	16.4	83.0
QM_1/8	n.d.	n.d.	n.d.	7.8	70.0
octM	3.4	2.0	9.5 [c]		
QoctM_1/2	2.8	1.7	28.2	33.9	100.0
QoctM_1/4	1.9	2.6	17.4	18.9	95.7
QoctM_1/8	n.d.	n.d.	n.d.	8.2	74.2

n.d. = not determined

[a] Measured in the 30 – 100 °C range. [b] Measured in the 800 – 1000 °C range, before isotherm in air. [c] Octyl functionalities. [d] Remaining weight loss other than [a] and [b], and also [c] in the case of QoctM complexes. [e] Measured by UV-Vis spectrophotometer.

The calculated values are in good agreement with Q quantification by UV-Vis spectroscopy after extraction with absolute methanol (Table 2). These values were double checked by measuring the Q amount remained in the supernatant (not reported). Table 2 also shows the encapsulation efficiency (% EE) that is the amount of Q included in the silica mesopores with respect to the totally employed. On the basis of these results it can be stated that the complexation by the kneading method gave the most satisfactory results in terms of both loading and encapsulation efficiency by employing octM matrix, particularly at low organic/inorganic weight ratio.

From a molecular point of view, these results can be explained in terms of the Q/silica interaction. In the case of QM complexes, the decrease of adsorbed water and of dehydroxylation

with respect to M matrix is in agreement with the formation of hydrogen bonding adducts of Q with surface Si-OH. On the contrary, this is less evident for QoctM ones, where a more lipophilic environment is probably favoring van der Waals interaction between alkyl chains and Q aromatic rings. We can thus suppose that the higher loading and %EE measured in the latter case are the result of an interplay between hydrogen bonding with residual Si-OH (higher interaction strength but smaller amount) and van der Waals forces (weaker but more abundant in number).

DSC thermograms obtained with M silica were similar to those obtained with octM silica, so they will be discussed together and for sake of clarity only the former ones are reported (Fig. 5). Namely, bare M did not display any peak while pure Q showed an intense endothermic peak at 320.50°C characterized by 112.3 J/g ΔH and related to the melting process. The lack of this peak in all the QM and QoctM complexes suggested the molecular dispersion of Q within the silica pores and an important Q/silica molecular interaction. In contrast, even if broadened and weaker, the melting peak is detectable in the thermograms of both QM and QoctM physical mixtures. However these lower peaks ($16.2<\Delta H<22.1$) were shifted to 230-280 °C range suggesting a certain degree of interaction occurred also for simple physical mixture.

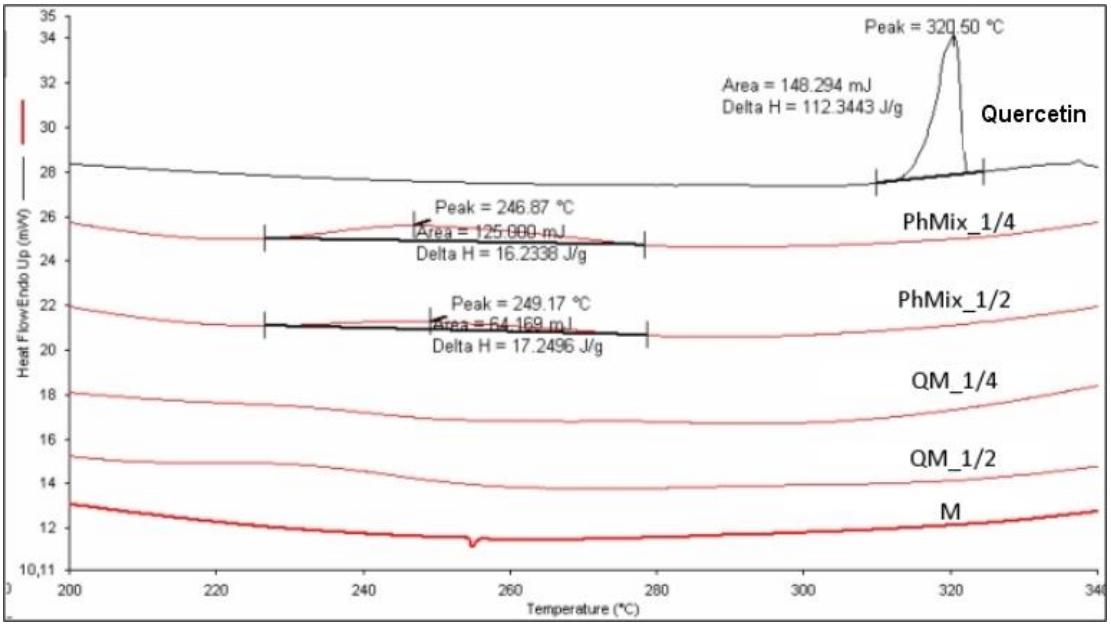

Fig. 5. DSC thermograms of Q, M, QM_1/2 and QM_1/4 complexes and their respectively physical mixtures.

IR spectroscopy was employed to get information on the interaction of Q with the silica surface at a molecular level, as shown in Fig. 6 for the 1/4 samples. For easier comparison, the spectra of M parent sample is only reported in the high frequency region (top panel), where the typical O-H stretching mode (ν O-H) of isolated surface Si-OH groups can be observed at 3745 cm^{-1}. Moreover, the weak component at 3715 cm^{-1}, and the broad adsorption centered at 3500 cm^{-1} on sample M can be assigned to Si-OH groups involved in acceptor and donor hydrogen bonding, respectively, together with hydroxyl groups of adsorbed water [46-48]. The intensity of the band at 3745 cm^{-1} is halved on octM sample, confirming the occurred condensation of surface Si-OH groups with the octyl alkoxide. This is supported by the appearance of strong bands in the 3000 – 2800 cm^{-1} range, assigned to ν C-H modes of the alkyl chains.

The IR spectrum of Q molecule in the high frequency region (curve e) is not particularly informative, being characterized by a weak band at 3592 cm^{-1}, and by a broad absorption extending from 3500 to 2800 cm^{-1}, with components at 3366 and 3318 cm^{-1}. These features are assigned to the νO-H of free and intermolecular hydrogen bonded OH groups, respectively. The expected νC-H

modes of the aromatic ring are hardly observable, excepted for a weak feature at 3090 cm^{-1}, being overlapped by the hydrogen bonding absorption. As a consequence, the spectra of QM_1/4 and QoctM_1/4 complexes in this region are dominated by the signals related to free and hydrogen bonded Si-OH. It is noticeably that in both cases the band at 3745 cm^{-1} due to isolated Si-OH is consumed after Q inclusion, with a corresponding increase of the broad band between 3700 and 3000 cm^{-1}, due to hydrogen bonded species. This implies that Q molecules are interacting with the silica surface through hydrogen bonding via the Si-OH groups, also in the presence of the octyl functionalities. In this case (sample QoctM_1/4, curve d) the absorption due to hydrogen bonded adducts is particularly intense and shifted to lower energy (maximum at 3380 cm^{-1}) with respect to the other samples. This suggest that the surface functionalization, meant to increase the surface lipophilicity, also caused an increase in the Brønsted strength of isolated Si-OH groups, in agreement with recent reports [49].

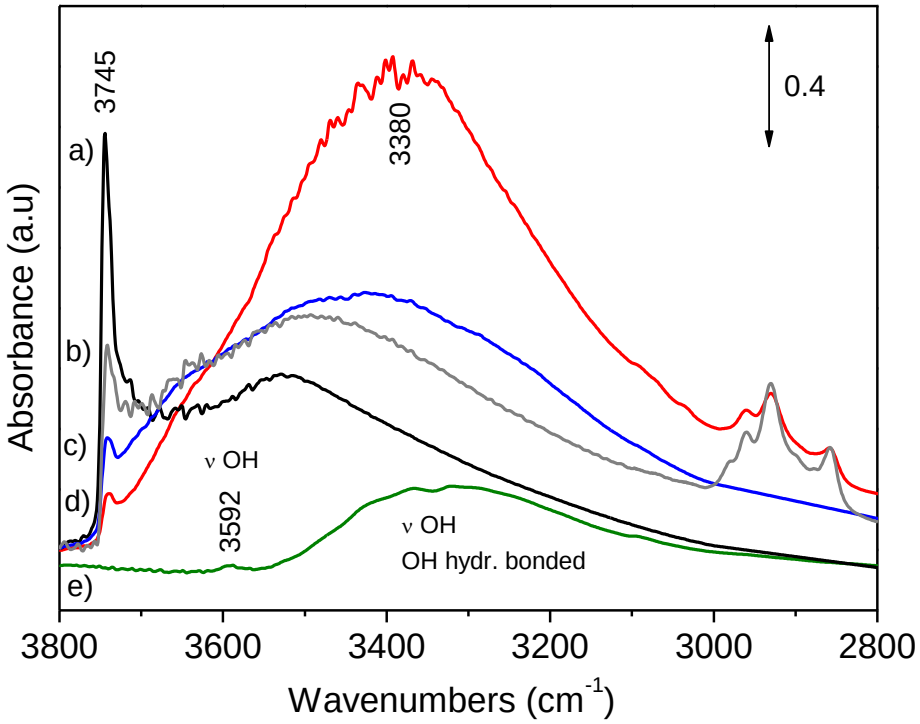
3745
3380
0.4
a)
b)
c)
d)
e)
ν OH
3592
ν OH
OH hydr. bonded
Absorbance (a.u)
3800
3600
3400
3200
3000
2800
Wavenumbers (cm-1)

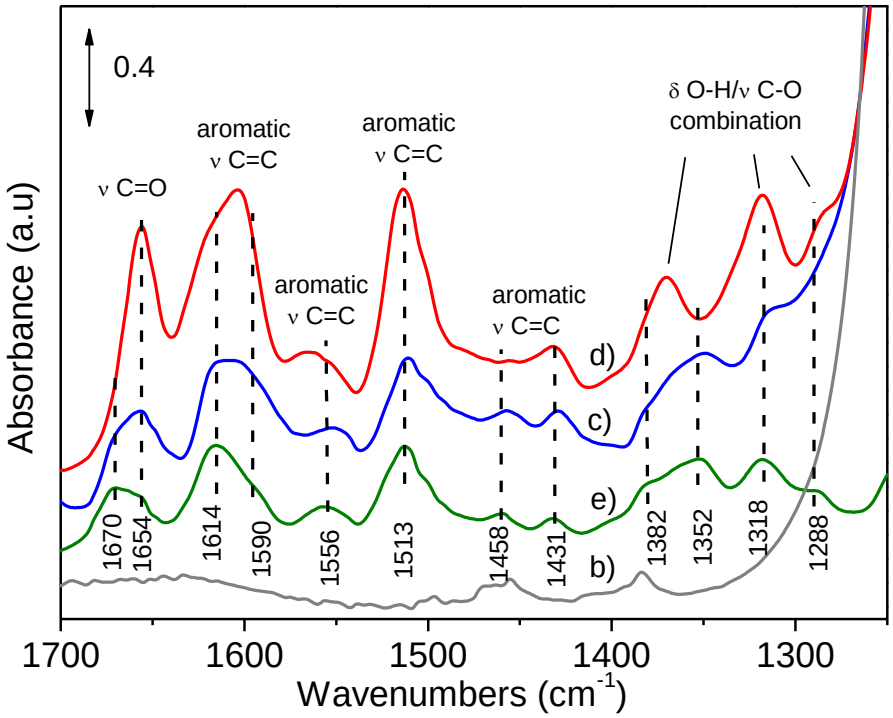
0.4
ν C=O
aromatic
ν C=C
aromatic
ν C=C
aromatic
ν C=C
aromatic
ν C=C
δ O-H/ν C-O
combination
d)
c)
e)
b)
1670
1654
1614
1590
1556
1513
1458
1431
1382
1352
1318
1288
Absorbance (a.u)
1700
1600
1500
1400
1300
Wavenumbers (cm-1)

Fig. 6. FTIR spectra of: a) M; b) octM; c) QM_1/4; d) QoctM_1/4; e) Q. Top and bottom: high and low frequency ranges, respectively. Samples were measured after RT outgassing, Q was measured in KBr. Spectra of M is reported for comparison only in the high frequency range.

Additional information about Q molecules in the complexes can be obtained by accurate analysis of low energy region (Fig. 6, bottom panel). In this case only the spectrum of octM was reported for comparison, showing the typical bending modes of CH_2 and CH_3 groups (δC-H, 1497, 1457 and 1384 cm^{-1}) of the octyl functionality, superimposed to the broad bands due to the overtone and combination modes of silica [46].

The spectrum of solid state Q molecules (curve e) shows the typical modes of νC=O (1670 and 1654 cm^{-1}), the νC=C of the aromatic rings (between 1640 and 1400 cm^{-1}) and the combination of νC-O and δO-H modes between 1400 and 1300 cm^{-1}. It is noticeable that some of these bands are asymmetric, indicating the presence of different conformations of the molecule, as expected when intermolecular interactions are taking place. This is particularly evident for the νC=O band, showing two components at 1670 and 1654 cm^{-1}, and for the bands at 1382 and 1352 cm^{-1}, related to the O-H groups. The asymmetric character of the aromatic νC=C at 1614/1590 and 1513 cm^{-1} (shoulder at 1500 cm^{-1}), cannot be easily rationalized, since these components are affected by the rings substitution [50].

All the mentioned bands are present on QM_1/4 and QoctM_1/4 complexes, with significant changes in shape and relative intensity. As for QM_1/4 the main changes involve the νC=O band and the aromatic νC=C at 1614 and 1590 cm^{-1} (spectrum c). The former indicates the presence of different conformations of Q molecules also after inclusion within the silica pores, suggesting that intermolecular interaction are still taking place, probably through dimers. The latter suggests the involvement of aromatic rings in the formation of hydrogen-bonded adducts with surface Si-OH.

Interestingly, the spectrum of Q is simplified when occluded in octM (spectrum d), particularly in the region related to νC=O and to the combination νC-O/δO-H modes, where sharp

bands are observed at 1654, 1368 and 1314 cm^{-1}. As for the aromatic νC=C at 1614 and 1590 cm^{-1}, their relative intensity is affected in a greater degree with respect to QM_1/4. We also acknowledge a higher intensity of the whole spectrum, not completely explained on the basis of the Q loading measured by TGA and by UV-Vis spectroscopy. These evidences suggest a more homogeneous distribution of Q molecules, which can be considered as isolated moieties, directly interacting with surface Si-OH groups through the phenyl and/or phenol O-H groups. We can thus infer that the octyl chains play a major role in diluting/physically separating Q molecules within the silica pores.

3.2 Testing of complex properties

QM_1/X and QoctM_1/X complexes were evaluated for their properties, stability and antioxidant activity *in vitro* by employing different methods and comparing the results with pure Q.

Diffusion runs through a semi-permeable cellulose membrane were carried out in order to foresee Q release from the mesoporous matrices. Artificial membranes have been often used to study both transdermal and dermal drug permeation [51]. In particular cellulose membranes, traditionally employed for dialysis, have more recently been applied to measure drug diffusion, to determine drug release rates from topical formulations and to screen such formulations as ointments, creams and hydrogels [52].

As an example in Fig. 7 QM and QoctM complexes prepared at 1/4 w/w ratio were compared with pure Q in terms of diffusion. Q release rates were estimated from the equations obtained by linearizing the diffusion profiles arbitrarily starting from the first hour (see Table 3). Overall, as expected, Q diffusion from the complexes was significantly slower than from the equivalent donor phase with pure Q testifying an important organic/inorganic interaction. However, by passing from 1/2 to 1/8 ratio the diffusion delay decreased in line with reduced Q loading values found both in QM_1/8 and in QoctM_1/8.

Noticeably, QoctM_1/X complexes, which exhibited Q loading values higher than corresponding QM_1/X (see Table 2), also showed higher diffusion delays. Moreover, in contrast to

QM complexes, QoctM ones, more precisely 1/2 and 1/4 w/w, presented a lag time in their diffusion profiles of 1 h and 2 h, respectively. These trends are in agreement with the characterization results, particularly IR, that suggest a stronger hydrogen bonding interaction with surface Si-OH, and the involvement of additional van der Waals interactions with octyl chains in functionalized octM matrix.

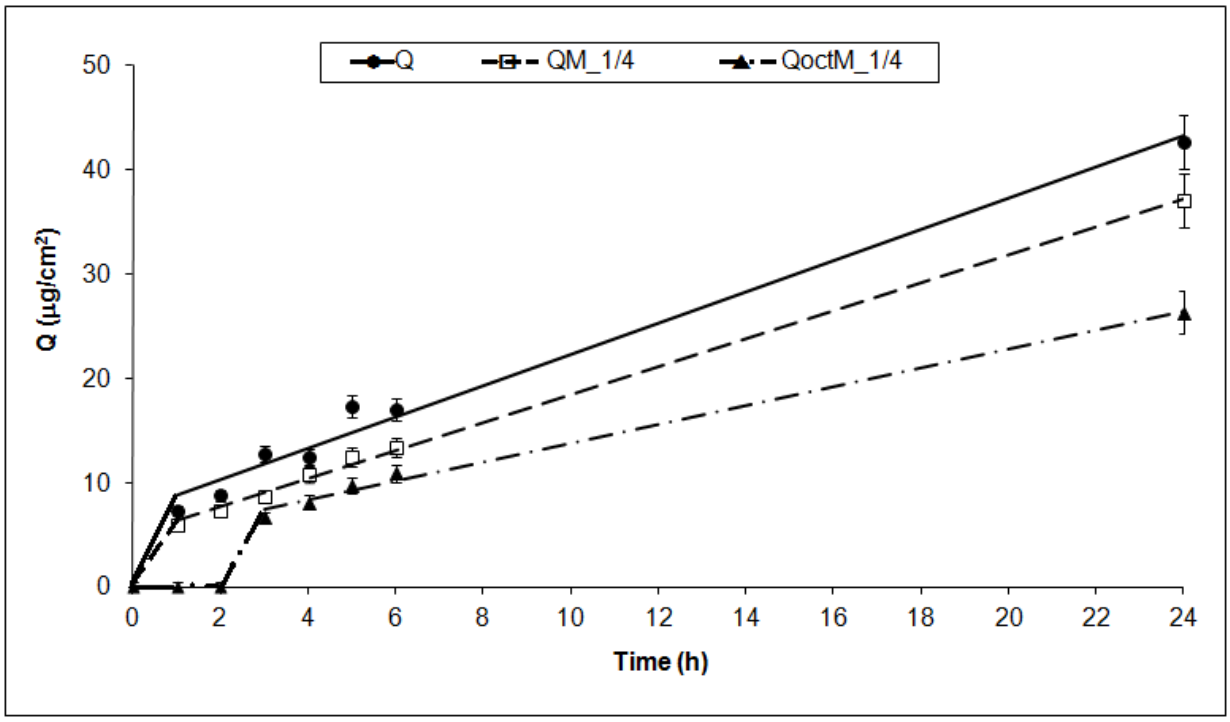

Fig. 7. Diffusion profiles of Q (solid line, circle), QM_1/4 (dotted line, square) and QoctM_1/4 (dotted and dashed line, triangle) through the cellulose membrane. Each bar represents the mean ± SD obtained in three independent experiments (n=3).

Table 3. Amounts (after 1 h) and rate equations of Q diffused through the cellulose membrane

Samples	Q (μg/cm^2) after 1 h diffusion	Equations and R^2 values
Q	7.28	y = 1.50x + 7.26 (R^2 0.984)
QM_1/2	6.66	y = 1.19x + 7.13 (R^2 0.986)
QM_1/4	5.86	y = 1.34x + 5.01 (R^2 0.998)
QM_1/8	6.38	y = 1.50x + 6.09 (R^2 0.996)
QoctM_1/2 [a]	0	y = 0.78x + 5.90 (R^2 0.948)
QoctM_1/4 [b]	0	y = 0.91x + 4.72 (R^2 0.995)
QoctM_1/8	5.95	y = 1.28x + 5.65 (R^2 0.995)

[a] Lag time = 1 h. Equation calculated in the 2-24 h interval. [b] Lag time = 2 h. Equation calculated in the 3-24 h interval.

The photostability over time of Q, free or immobilized in mesoporous silica, was tested in order to evaluate the protective potentiality of these matrices toward UV-induced degradation phenomena. In these experiments two different dispersion media containing TiO_2 were employed; this oxide is an inorganic filter that elsewhere showed photocatalytic properties promoting the transformation of organic molecules upon UV irradiation [53]. Firstly, a hydroalcoholic solution with 0.05% w/w TiO_2 was chosen for a preliminary screening, secondly an O/W emulsion at pH 5.0 containing a higher TiO_2 percentage (1.0% w/w) was selected as more representative of commercial suncare products. The photodegradation curves were linearized (Fig. 8 and 9) and the rate equations were reported in Table 4 and 5.

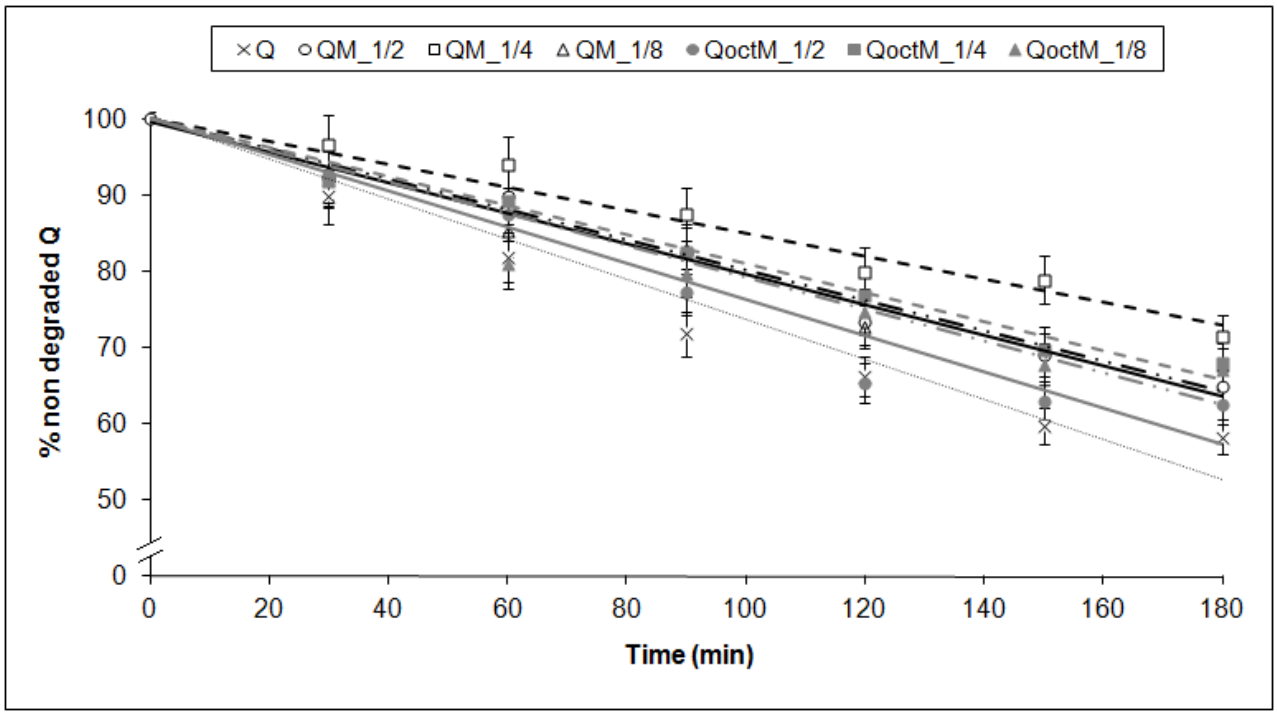

Fig. 8. Photodegradation kinetics of Q, free (thin line) or complexed with M (dark line) or octM (grey line), in different w/w ratio: 1/2 (solid), 1/4 (dotted), 1/8 (dotted and dashed) in ethanol/water (15/85 v/v), upon UVB irradiation (3 h). Each bar represents the mean ± SD obtained in three independent experiments (n=3).

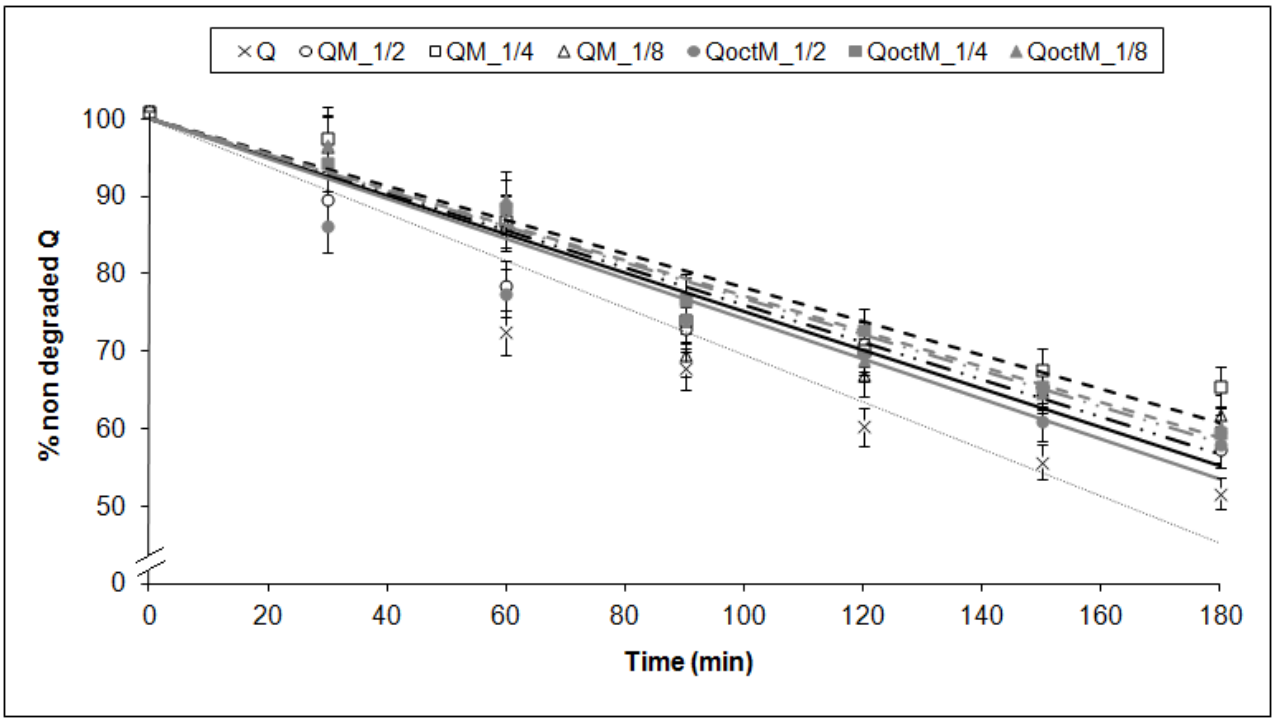

Fig. 9. Photodegradation kinetics of Q, free (thin line) or complexed with M (dark line) or octM (grey line), in different w/w ratio: 1/2 (solid), 1/4 (dotted), 1/8 (dotted and dashed) in O/W emulsion at pH 5.0, upon UVB irradiation (3 h). Each bar represents the mean ± SD obtained in three independent experiments (n=3).

Table 4. Photodegradation equations of Q, free or complexed with silica in different w/w ratio, in ethanol/water (15/85 v/v) upon UVB irradiation (3 h)

w/w ratio	QoctM	QM	Q
1/2	y = -0.237x + 98.16 R^2 = 0.950	y = -0.202x + 99.67 R^2 = 0.956	
1/4	y = -0.190x + 97.76 R^2 = 0.979	y = -0.151x + 103.04 R^2 = 0.981	y = -0.263x + 93.33 R^2 = 0.939
1/8	y = -0.207x + 92.93 R^2 = 0.899	y = -0.198x + 96.45 R^2 = 0.955	

Table 5. Photodegradation equations of Q, free or complexed with silica in different w/w ratio, in O/W emulsion at pH 5.0 upon UVB irradiation (3 h)

w/w ratio	QoctM	QM	Q
1/2	$y = -0.259x + 89.13$ $R^2 = 0.909$	$y = -0.249x + 91.58$ $R^2 = 0.908$	
1/4	$y = -0.229x + 101.24$ $R^2 = 0.989$	$y = -0.218x + 99.03$ $R^2 = 0.928$	$y = -0.304x + 90.50$ $R^2 = 0.902$
1/8	$y = -0.232x + 102.91$ $R^2 = 0.960$	$y = -0.241x + 98.20$ $R^2 = 0.913$	

The obtained values of regression coefficient (R^2) indicated that pseudo-zero order suitably described the trends of photodegradation. Data also showed that the best-fit degradation kinetics with the highest value of R^2 was shown by 1/4 complexes. By comparing the equations it is possible to observe for all the tested complexes, in both the dispersion media, a slight decrease in the slope indicating that the inclusion of Q in silica pores results in a certain photoprotection. Unexpectedly, equations show that silica functionalization did not significantly influence the degree of protection. This could be explained as a result of Q diffusion from the silica pores to the dispersion media during the irradiation tests.

From the reported data it can be also observed that despite the higher amount of titania employed in the emulsion system, the rates of Q degradation were comparable to those obtained with the aqueous solution suggesting an important protective effect of this medium probably related to its less polar and more organized structure. In our previous work [54], similarly MCM-41 resulted photoprotective with respect to the free guest molecule particularly in the emulsion where the complexes were supposed to be confined at the O/W interface.

As regards the storage stability in dark condition at 37 °C (see Table 6) it can be noted that the immobilization in silica matrices significantly reduced the decrease of Q concentration over time; this was especially evident for QoctM complexes. Interestingly, the degradation trend decreased by

decreasing the pH value of the dispersion media for all the tested samples: after 180 min the percentage of non degraded Q resulted 59.2% at physiological pH and 83.1% at acid pH, respectively. Similar results were obtained with the complexes: at the end of the experiment, passing from 7.4 to 5.0 pH, the remaining percentages of Q were respectively 82.4% and 95.4% with QoctM_1/4 while 72.1% and 91.5% with QM_1/4. In all cases mesoporous silica, especially octM, played a key role in preventing guest degradation during storage experiment.

Table 6. Percentage of non-degraded Q, free or complexed with silica in 1/4 w/w ratio, in ethanol/citrate buffer (15/85 v/v, pH 5.0) or in ethanol/phosphate buffer (15/85 v/v, pH 7.4) after 90 and 180 min of dark storage at 37 °C

Samples	pH 5.0		pH 7.4	
	90 min	180 min	90 min	180 min
QoctM_1/4	97.7%	95.4%	85.3%	82.4%
QM_1/4	97.6%	91.5%	85.0%	72.1%
Q	95.0%	83.1%	73.0%	59.2%

In this work the DPPH• assay was used in order to study if the complexation of Q modifies its antioxidant behavior. Radical scavenging activity is very important, due to the deleterious role of free radicals in biological systems. The ability of polyphenolic compounds to act as antioxidants depends on the redox properties of their phenolic hydroxyl groups and the potential for electronic delocalization across the chemical structure. Several methods are currently used to assess antioxidant activity of plant phenolic compounds. DPPH• assay is considered a valid, easy and high sensitive method to evaluate the RSA of antioxidants [55]. The free radical DPPH• shows an absorption peak around 515 nm, which decreases when DPPH• is scavenged by an antioxidant through donation of hydrogen to form the corresponding hydrazine. Fig. 10 shows % RSA of Q, QM_1/4 and QoctM_1/4 at different levels of concentration. This assay was also detected on

mesoporous silica alone in order to investigate if M and octM could interfere, confirming that silica did not interfere with the DPPH• assay. In agreement with the literature report [56], linear correlations for Q concentration vs. % RSA were obtained. Moreover, while not always in a significant amount, complexation of Q (particularly with unfunctionalized silica) increased slightly the efficacy of the antioxidant at low levels. Overall, results from this assay may be explained based on the accessibility of the antioxidant to the DPPH• radical combined with the stability of the antioxidant free-radical following hydrogen abstraction by DPPH•. Furthermore, this assay confirmed that Q structure was preserved in the complexes, as already assessed by FTIR analysis.

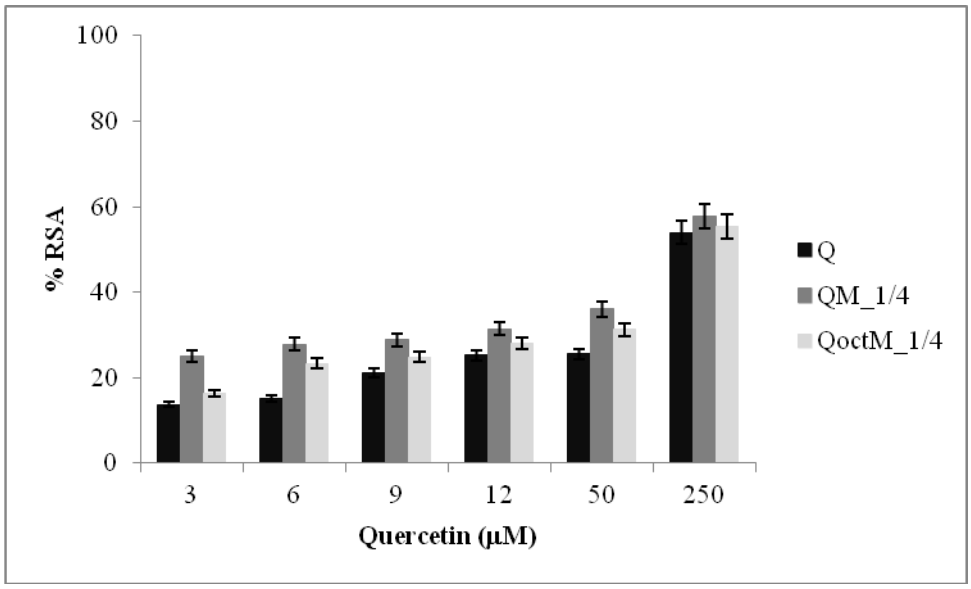

Fig. 10. Antiradical activity (expressed as % RSA) of free Q, QM_1/4 and QoctM_1/4 towards DPPH•. Each bar represents the mean ± SD obtained in three independent experiments (n=3).

Antioxidant metal chelating capacity is significant, since it reduces the concentration of the catalyzing transition metal in lipid peroxidation. The importance of metal chelating is often neglected, but trace metals significantly contribute to the free radical formation by decomposition of lipid hydroperoxides into free radicals. In this assay metal chelating activity was assessed using ferrozine, a strong chelator that can quantitatively form red complexes with Fe^{2+}. In the presence of

chelating agents, the complex formation is disrupted and a decrease in the red color is observed; measurement of color reduction, therefore, allows estimation of the metal chelating activity of the coexisting chelator. Lower absorbance indicates higher metal chelating activity. In according with the literature [57], Q interfered with the formation of the ferrous-ferrozine complex (Fig. 11) suggesting that Q had chelating activity and was able to capture ferrous ions before ferrozine. Our hypothesis is that Q structure should bind metal cations through three different sites, either on 3-hydroxychromone or on 5-hydroxychromone functions or on hydroxyl groups of the catechol moiety, as suggested by other authors [58]. At the same time, QM_1/4 and QoctM_1/4 exhibited very similar binding capacities; moreover in the figure it is also possible to observe that in all cases the complexes, QoctM in particular, showed a slightly higher reducing ability, *i.e.* the complexes behaved as better antioxidants than polyphenol alone. Metal chelating activity both in Q and in complexes was concentration dependent. The maintenance of the ability to form iron complexes is an important attribute for silica complexes because free transition metals like iron react with either hydrogen or lipid peroxides to produce hydroxyl radical compounds and alkoxyl radicals, also known as the Fenton reaction [59]. These radicals are extremely reactive and will significantly accelerate oxidative degradation processes as well as unpleasant smell. When iron ions are chelated, they may lose their pro-oxidant properties; ferrous chelation may provide important antioxidative effects by retarding metal-catalyzed oxidation. Similarly to DPPH$^{\bullet}$ test, this assay was also detected on mesoporous silica alone in order to investigate if M and octM could interfere, confirming that silica alone did not show chelation activity.

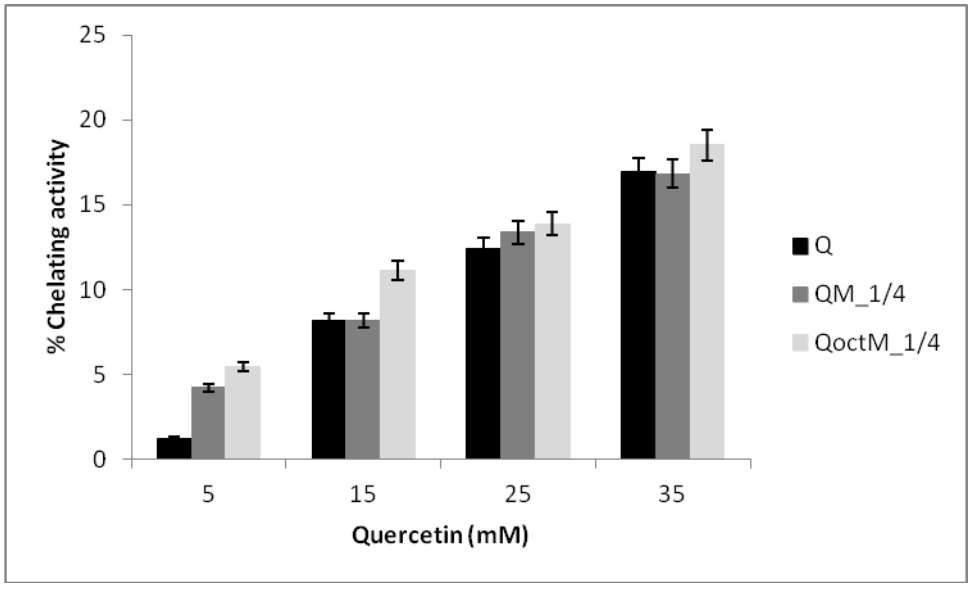

Fig. 11. Chelating activity percentage of free Q, QM_1/4 and QoctM_1/4. Each bar represents the mean ± SD obtained in three independent experiments (n=3).

4 Conclusions

The immobilization of quercetin (Q) in the mesoporous inorganic matrix by a kneading method successfully stabilized this flavonoid improving its antioxidant efficacy. Notably, this technique offered the advantage of short preparation time, high recovery and guest loading. The hydrophilic/lipophilic character of MCM-41 was also modulated by functionalizing the silica surface with octyl chains. Important organic/inorganic interactions were confirmed suggesting a certain affinity between Q and silica. More in detail, IR spectroscopy showed the formation of hydrogen bonded adducts with silica Si-OH groups in both matrices, irrespective of surface functionalization. However, detailed spectral analysis suggests that in octM matrix Q molecules are more dispersed and form stronger hydrogen bonded adducts with residual Si-OH. We can thus infer that octyl chains play an important role in diluting Q molecules within the silica pores and in stabilizing the interaction with the surface through lateral van der Waals interactions.

The studies of diffusion through a semi-permeable membrane reveled a slower release of Q from the complexes with respect to the free molecule, further confirming the successful host/guest interaction.

It is interesting to note that when exposed to UV irradiation the mesoporous silica significantly improved Q stability over time indicating a certain capacity in preserving the efficacy against skin damage. Noticeably, the protection appears to be correlate with the physico-chemical characteristics of the surroundings (i.e. the presence of alkyl chains on the silica surface, the occurrence of an O/W interface and the pH of the dispersion medium) emphasizing the role of colloid and interface on the antioxidant effectiveness. Specifically, the major complex stability was observed at pH 5.0 that fits perfectly the skin pH value suggesting the advantageous applicability of MCM-41 as carrier in the topical field. Moreover the Q immobilization in MCM-41 matrices not only maintained but even slightly enhanced its antiradical and metal-chelating activities.

The present work proposes a novel antioxidant carrier with performances comparable to those of other more common systems like liposomes, nanostructures or cyclodextrins [8,10,11]. Interestingly, Q/MCM-41 complexes show high loading values and a remarkable efficiency of encapsulation, further increased by the easily achieved silica functionalization [21].

In this research the innovative application of a model mesoporous complex in dermal delivery has been investigated, and considering the positive results it may be reasonably employed with other active molecules for which the use is limited by degradation phenomena.

Acknowledgments

Compagnia di San Paolo and University of Turin are gratefully acknowledged for funding Project ORTO114XNH through "Bando per il finanziamento di progetti di ricerca di Ateneo - anno 2011". Prof. S. Coluccia and Prof. M.E. Carlotti are gratefully acknowledged for fruitful discussion.

References

[1] B. Halliwell, Am. J. Med. 91 (1991) S14.

[2] H. Sies, Angew. Chem. Int. Edit. 25 (1986) 1058.

[3] H. Sies, Am. J. Med. 91 (1991) S31.

[4] H. Sies, Eur. J. Biochem. 215 (1993) 213.

[5] H. Ohshima, Y. Yoshie, S. Auriol, I. Gilibert, Free Radical Biol. Med. 25 (1998) 1057.

[6] T. Miyake, T. Shibamoto, J. Agric. Food Chem. 45 (1997) 1819.

[7] M. L. Calabro, S. Tommasini, P. Donato, D. Raneri, R. Stancanelli, P. Ficarra, R. Ficarra, C. Costa, S. Catania, C. Rustichelli, G. Gamberini, J. Pharm. Biomed. Anal. 35 (2004) 365.

[8] G. Wang, J. J. Wang, L. P. Zhang, S. M. Du, J. Y. Liu, L. Wang, F. Ye, Expert Opin. Drug Deliv. 9 (2012) 599.

[9] C.-H. Choi, S.-H. Kim, S. Shanmugam, R. Baskaran, J.-S. Park, C.-S. Yong, H.-G. Choi, B.-K. Yoo, K. Han, Biomol. Ther. 18 (2010) 99.

[10] G. Chen-yu, Y. Chun-fen, L. Qi-lu, T. Qi, X. Yan-wei, L. Wei-na, Z. Guang-xi, Int. J. Pharm. 430 (2012) 292.

[11] M. E. Carlotti, S. Sapino, E. Ugazio, G. Caron, J. Incl. Phenom. Macrocycl. Chem. 70 (2011) 81.

[12] S. Sapino, M. E. Carlotti, R. Cavalli, M. Trotta, F. Trotta, D. Vione, J. Incl. Phenom. Macrocycl. Chem. 57 (2007) 451.

[13] U. Costantino, V. Ambrogi, M. Nocchetti, L. Perioli, Microporous Mesoporous Mater. 107 (2008) 149.

[14] Y. Kohno, K. Totsuka, S. Ikoma, K. Yoda, M. Shibata, R. Matsushima, Y. Tomita, Y. Maeda, K. Kobayashi, J. Colloid Interface Sci. 337 (2009) 117.

[15] V. Ambrogi, L. Perioli, F. Marmottini, L. Latterini, C. Rossi, U. Costantino, J. Phys. Chem. Solids 68 (2007) 1173.

[16] T. Itoh, K. Yano, Y. Inada, Y. Fukushima, J. Am. Chem. Soc. 124 (2002) 13437.

[17] O. A. Kazakova, V. M. Gun'ko, N. A. Lipkovskaya, E. F. Voronin, V. K. Pogorelyi, Colloid J. 64 (2002) 412.

[18] T. V. Fedyanina, V. N. Barvinchenko, N. A. Lipkovskaya, V. K. Pogorelyi, Colloid J. 70 (2008) 215.

[19] C. T. Kresge, M. E. Leonowicz, W. J. Roth, J. C. Vartuli, J. S. Beck, Nature 359 (1992) 710.

[20] M. Vallet-Regi, F. Balas, D. Arcos, Angew. Chem. Int. Edit. 46 (2007) 7548.

[21] M. Manzano, V. Aina, C. O. Arean, F. Balas, V. Cauda, M. Colilla, M. R. Delgado, M. Vallet-Regi, Chem. Eng. J. 137 (2008) 30.

[22] W. Whitnall, T. Asefa, G. A. Ozin, Adv. Funct. Mater. 15 (2005) 1696.

[23] A. Wada, S. Tamaru, M. Ikeda, I. Hamachi, J. Am. Chem. Soc. 131 (2009) 5321.

[24] X. S. Zhao, X. Y. Bao, W. P. Guo, F. Y. Lee, Mater. Today 9 (2006) 32.

[25] S. Hudson, J. Cooney, E. Magner, Angew. Chem. Int. Edit. 47 (2008) 8582.

[26] M. Hartmann, Chem. Mater. 17 (2005) 4577.

[27] L. Giussani, E. Fois, E. Gianotti, G. Tabacchi, A. Gamba, S. Coluccia, ChemPhysChem 11 (2010) 1757.

[28] H. G. Manyar, E. Gianotti, Y. Sakamoto, O. Terasaki, S. Coluccia, S. Tumbiolo, J. Phys. Chem. C 112 (2008) 18110.

[29] S. M. Zhu, Z. Y. Zhou, D. Zhang, ChemPhysChem 8 (2007) 2478.

[30] E. Gianotti, C. A. Bertolino, C. Benzi, G. Nicotra, G. Caputo, R. Castino, C. Isidoro, S. Coluccia, ACS Appl. Mater. Interfaces 1 (2009) 678.

[31] S. H. Wu, Y. S. Lin, Y. Hung, Y. H. Chou, Y. H. Hsu, C. Chang, C. Y. Mou, ChemBioChem 9 (2008) 53.

[32] V. S. Y. Lin, C. Y. Lai, J. G. Huang, S. A. Song, S. Xu, J. Am. Chem. Soc. 123 (2001) 11510.

[33] Y. W. Chen-Yang, Y. T. Chen, C. C. Li, H. C. Yu, Y. C. Chuang, J. H. Su, Y. T. Lin, Mater. Lett. 65 (2011) 1060.

[34] D. N. Bikiaris, Expert Opin. Drug Deliv. 8 (2011) 1663.

[35] L. P. V. Calsavara, G. M. Zanin, F. F. de Moraes, J. Incl. Phenom. Macrocycl. Chem. 73 (2012) 219.

[36] J. S. Beck, J. C. Vartuli, W. J. Roth, M. E. Leonowicz, C. T. Kresge, K. D. Schmitt, C. T. W. Chu, D. H. Olson, E. W. Sheppard, J. B. McCullen, J. B. Higgins, J. L. Schlenken, J. Am. Chem. Soc. 114 (1992) 10834.

[37] J. Choma, M. Jaroniec, W. Burakiewicz-Mortka, M. Kloske, Appl. Surf. Sci. 196 (2002) 216.

[38] I. Gulcin, Life Sci. 78 (2006) 803.

[39] T. C. P. Dinis, V. M. C. Madeira, L. A. Almeida, Arch. Biochem. Biophys. 315 (1994) 161.

[40] A. Molinari, A. Maldotti, A. Bratovcic, G. Magnacca, Catal. Today 161 (2011) 64.

[41] Grosman Annie, O. Camille, Langmuir 21 (2005) 10515.

[42] L. D. Gelb, Mol. Phys. 100 (2002) 2049.

[43] K. Sing, D. Everett, R. HAUL, L. Moscou, R. Pierotti, J. Rouquerol, T. Siemieniewska, Pure Appl. Chem. 57 (1985) 603.

[44] M. Kruk, M. Jaroniec, Chem. Mater. 13 (2001) 3169.

[45] S. A. Kozlova, S. D. Kirik, Microporous Mesoporous Mater. 133 (2010) 124.

[46] A. Zecchina, S. Bordiga, G. Spoto, L. Marchese, G. Petrini, G. Leofanti, M. Padovan, J. Phys. Chem. 96 (1992) 4991.

[47] S. Tosoni, B. Civalleri, F. Pascale, P. Ugliengo, J. Phys.: Conf. Ser. 117 (2008) 1.

[48] I. Braschi, G. Gatti, C. Bisio, G. Berlier, V. Sacchetto, M. Cossi, L. Marchese, J. Phys. Chem. C 116 (2012) 6943.

[49] J.-P. Dacquin, H. E. Cross, D. R. Brown, T. Duren, J. J. Williams, A. F. Lee, K. Wilson, Green Chem. 12 (2010) 1383.

[50] G. Socrates, *Infrared and Raman characteristic group frequencies*. Third edition ed.; John Wiley & Sons Ltd: Chichester, England, 2006.

[51] M. Trotta, E. Ugazio, E. Peira, C. Pulitano, J. Control. Release 86 (2003) 315.

[52] S. Fiala, M. B. Brown, S. A. Jones, J. Pharm. Pharmacol. 60 (2008) 1615.

[53] M. E. Carlotti, E. Ugazio, S. Sapino, I. Fenoglio, G. Greco, B. Fubini, Free Radical Res. 43 (2009) 312.

[54] L. Gastaldi, E. Ugazio, S. Sapino, P. Iliade, I. Miletto, G. Berlier, Phys. Chem. Chem. Phys. 14 (2012) 11318.

[55] C. Sànchez-Moreno, Food Sci. Technol. Int. 8 (2002) 121.

[56] B. Yang, A. Kotani, K. Arai, F. Kusu, Anal. Sci. 17 (2001) 599.

[57] M. Guo, C. Perez, Y. Wei, E. Rapoza, G. Su, F. Bou-Abdallah, N. D. Chasteen, Dalton Trans. 43 (2007) 4951.

[58] S. Fiorucci, J. Golebiowski, D. Cabrol-Bass, S. Antonczak, J. Agric. Food Chem. 55 (2007) 903.

[59] K. Le, F. Chiu, K. Ng, Food Chem. 105 (2007) 353.